Simulation of an Ablative Thermal Protection System for the Hypersonic Ascend of an Electromagnetically Launched Payload Carrier

Daniel Lancelle and Ognjan Božić**
**German Aerospace Center Institute of Aerodynamics and Flow Technology*
Lilienthalplatz 7, 38108 Braunschweig, Germany

Abstract

The German Aerospace Center is carrying out a study to develop a small payload carrier for the ascent to low earth orbit. The vehicle shall be electromagnetically launched by a Lorentz Rail Accelerator. Additionally, it will be propelled by a two stage hybrid rocket engine system to reach the desired orbit. Due to the high initial velocity of about 3.3 km/s at sea level, the vehicle needs a thermal protection system to withstand the aerothermodynamic loads on its forebody. An ablative carbon phenolic heat shield is chosen for this application. There are many investigations regarding carbon phenolic ablators, but usually these investigations are carried out for re-entry missions, where the high velocities are given at high altitude and low atmospheric density, in contrast to this application.
A material response model is developed and coupled to a 6 degree of freedom trajectory simulation tool, which incorporates an aerodynamic and atmospheric model. The results show that despite the high convective heat loads, an ablator of 15 mm thickness at the stagnation region is sufficient to protect the vehicle against the harsh conditions.

Abbreviations

DLR	- Deutsches Zentrum für Luft- und Raumfahrt	6-DOF	- 6 Degree of Freedom
LRA	- Lorentz Rail Accelerator	CFD	- Computational Fluid Dynamics
TPS	- Thermal Protection System	THERESA	- Thermal Response and Ablation

Symbols (Latin)

A	$[s^{-1}]$	Freq. Factor Pyrolysis React.
$\underline{\underline{A}}$	$[s^{-1}]$	Matrix
B	[-]	Blowing Parameter
$\underline{\underline{B}}$	[-]	Matrix
C	$[lb/(s \cdot ft^{3/2} \cdot atm^{1/2})]$	Mass Diffusion Constant
E	[J/mole]	Activation Energy
K	$[atm^{2/3}]$	Sublimation Constant
K_0	$[lb/(s \cdot ft^2 \cdot atm^{1/2})]$	Eff. Collision Frequency
M	[kg/mole]	Molar Mass
R	[J/(mol·K)]	Universal Gas Constant
St	[-]	Stanton Number
T	[K]	Temperature
c_p	[J/(kg·K)]	Specific Heat Capacity
h	[J/kg]	Specific Enthalpy
k	[W/(m·K)]	Thermal Conductivity
m	[kg]	Mass
$\dot{m}$	$[kg/(s \cdot m^2)]$	Mass Flux
p	$[N/m^2]$	Pressure
$\dot{q}$	$[W/m^2]$	Heat Flux
r	[m]	Radius
t	[s]	Time
u	[m/s]	Velocity
y	-	Wildcard for Set of Equations

Symbols (Greek)

ϕ	[-]	Stoichiometric Ratio
α	$[W/(m^2 \cdot K)]$	Coefficient of Heat Transfer
γ	$[s^{-1}]$	Matrix A Elements
δ	[m]	Length Increment
ε	[-]	Emissivity
ε	[-]	Implicit Scheme Coefficient
ρ	$[kg/m^3]$	Density
σ	$[W/(m^2 \cdot K^4)]$	Stefan-Boltzmann Constant
φ	[K/s]	Source Term

Indices

C	Carbon
O	Oxygen
R	Recovery
ad	Adiabatic
adj	Adjusted
b	Body
c	Char
cb	Combustion
char	Char

conv	Convective	rad	Radiative
corr	Corrected	req	Required
cw	Cold Wall	sub	Sublimation
diff	Diffusion	surf	Surface
e	Boundary Layer Edge	t	Time Derivative
gas	Gas	v	Virgin
i	Arbitrary Index	w	Wall
in	Input	x	Length Direction
j	Arbitrary Index	∞	Free Stream Condition
ox	Oxidation		

1. Introduction

The German Aerospace Center (DLR) is conducting a study to design and to optimize a small payload launcher that shall be electromagnetically launched by a Lorentz Rail Accelerator (LRA). The vehicle comprises of a hybrid rocket propulsion system for orbit injection. The use of an electrical acceleration system for a small payload carrier is a promising concept in the field of space transportation. By providing a part of the necessary launch energy as electrical energy, the fuel mass of a launch vehicle, and therefore its size, can be drastically reduced. Two DLR feasibility studies were dedicated to suborbital and orbital LRA-launched vehicles [1], [2].

From these studies one can derive a necessary launch velocity of about 3300 m/s. Due to this high velocity at low altitudes in the dense atmosphere, very high aerothermodynamics loads act upon the vehicle, especially on its forebody. To overcome these heat loads, a thermal protection system (TPS) is necessary to protect the vehicle during its flight through the atmosphere.

For the TPS a carbon phenolic ablative heat shield is chosen. It features a simple setup; it does not need active components, pipes or cooling media. It is the best choice for short time heat protection. Carbon phenolic charring ablators are well approved in re-entry applications and in the use as thermal protection for combustion chambers and nozzles of solid rocket motors and hybrid rocket engines. However, in this case the circumstances are different. During re-entry missions, there are high velocities given at high altitude and low atmospheric density, dissimilar to the ascend flight, where the highest velocity is given at sea level.

To assess whether an ablative heat shield can withstand the demands for an electromagnetically accelerated vehicle a material response model is developed that describes a carbon phenolic ablator mounted on a base structure. Thermal conductance, pyrolysis reaction, char erosion and pyrolysis gas production are taken into account. Furthermore, the conditions in the boundary layer near the stagnation point are modeled, including combustion of char and pyrolysis gas, blocking effect and radiation, to determine the heat flux to the ablator. The material response model is coupled to a 6 degree of freedom (6-DOF) trajectory simulation tool, which incorporates an aerodynamic and atmospheric model. Therefore, all aspects of the ascend flight can be investigated.

Figure 1: LRA Launched Payload Carrier

2. Thermal Protection System Model

A cross-section of a carbon phenolic heat shield is shown in Figure 2. The ablator, made from carbon fibres embedded in a phenolic resin is mounted on a base structure. The impinging heat flux from the inflow heats the material, until it undergoes a pyrolysis reaction. The virgin material is transformed to carbon char. As the pyrolysis zone penetrates the ablator, a char layer is formed, which again is eroded due to oxidation and sublimation. The gas produced by the pyrolysis reaction and the eroded char are injected into the boundary layer of the incoming flow. The pyrolysis reaction consumes energy and the mass injected into the boundary layer reduces the convective heat flux. These are the two main mechanism of thermal protection.

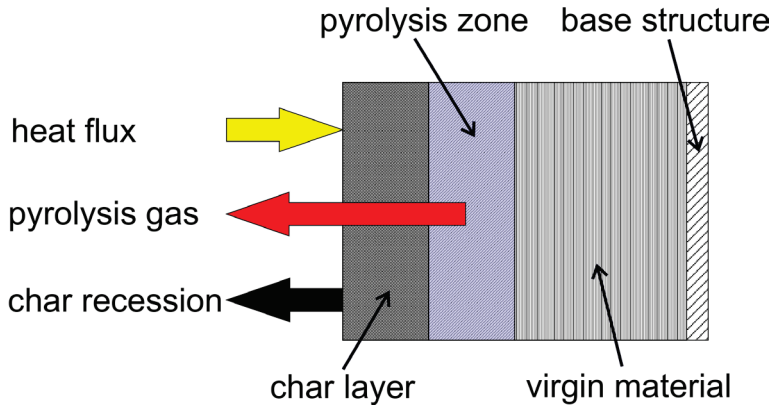

Figure 2: Charring Ablator

Within the software tool THERESA the TPS is simulated with a 1-D model comprising of the ablator and the base structure. The model takes into account the pyrolysis reaction, the thermal conduction in the material and the base structure, the impinging heat flux, and the interaction of the injected material with the boundary layer. The model is implemented using different engineering tools and avoiding CFD-techniques, to use it within a multi-disciplinary-optimization.

Figure 3 shows the computational sequence of one time step in the simulation. From a 6-DOF flight mechanics tool, trajectory data are provided to the TPS-model. Using the equations of Fay and Riddell [3] the convective cold wall heat flux to the stagnation point is calculated. Next, the amount of oxygen, that reaches the surface of the heat shield, is calculated. The surface recession and the decrease of convective heat flux due to blowing of material into the boundary layer are determined. In the next step, the combustion of char and pyrolysis gas within the boundary layer is calculated and the surface heat flux balance is derived. With the net heat flux entering the ablator, the heat conduction and pyrolysis reaction can be computed. The program is capable of computing the change of the surface geometry, which again influences the trajectory. However, this was not used for the simulations for this paper.

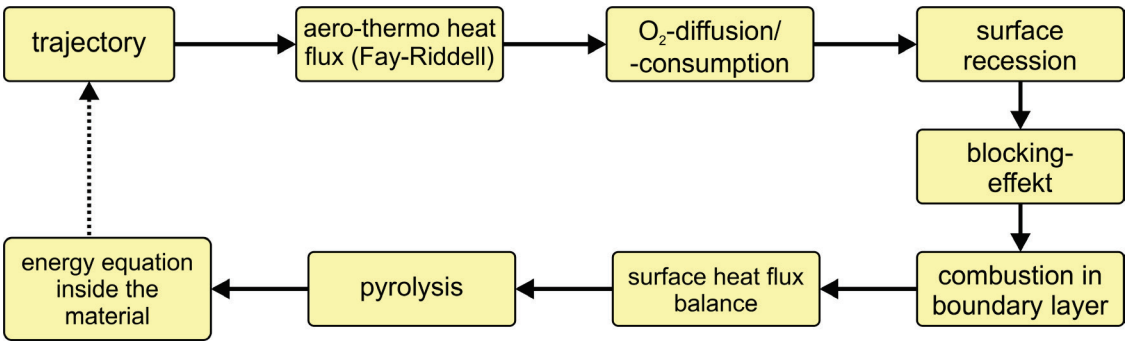

Figure 3: Flowchart of TPS Model

2.1 Heat Transfer

The convective cold wall heat flux is determined by means of the equations of Fay and Riddell [3]. The cold wall heat flux is reduced due to the pyrolysis gas and the surface material that is injected in the boundary layer due to char oxidation and sublimation. According to [4] the ratio of heat flux with blowing and cold wall heat flux can be determined as:

$$\frac{q_{conv}}{q_{conv,cw}} = 1 - 0.8\left(\frac{M_\infty}{M_{in}}\right)^{0.25} \cdot B + 0.13\left(\frac{M_\infty}{M_{in}}\right)^{0.5} \cdot B^2 . \quad \textbf{(1)}$$

B is the blowing factor. It can be derived from the mass flux that enters the boundary layer, the free stream density and the Stanton number:

$$B = \frac{\dot{m}_{gas} + \dot{m}_{char}}{\rho_\infty u_\infty St} . \quad \textbf{(2)}$$

Furthermore, the convective heat flux is increased due to combustion of pyrolysis gas and char. The combustion rate is assumed as infinity and the reaction shall be stoichiometric. Furthermore, the temperature dependence of the combustion enthalpy is neglected. The composition of the pyrolysis gas is assumed as constant. Depending on whether the combustion occurs at the surface or within the boundary layer, the heat flux is corrected as following:

$$\frac{\dot{q}_{conv,cb}}{\dot{q}_{conv}} = \frac{\left(h_{ad,w} - h_w\right) + 0.21 \cdot h_{cb}\left(\frac{\dot{m}_{cb}}{\dot{m}_{ox}}\right)_{\Phi=1}}{\left(h_{ad,w} - h_w\right)} , \quad \textbf{(3)}$$

$$\frac{\dot{q}_{conv,cb}}{\dot{q}_{conv}} = 1 + \dot{m}_{cb} h_{cb} . \quad \textbf{(4)}$$

Equation (3) is valid for combustion within the boundary layer [5]. The adiabatic wall enthalpy is increased by the amount of combustion enthalpy of the ablation products. For the combustion at the surface, it is assumed that the whole enthalpy of combustion is transferred to the surface (equation (4)).
In addition to the convective heat flux, the radiative heat flux and the heat flux due to sublimation of the char layer have to be taken into account. The radiative heat flux depends on the surface temperature and the emissivity (typical ε= 7.725 [10]):

$$\dot{q}_{rad} = \sigma \cdot \varepsilon \cdot T_w^4 . \quad \textbf{(5)}$$

The heat flux due to sublimation depends on the mass flux of subliming char and the specific enthalpy of sublimation:

$$\dot{q}_{sub} = \dot{m}_{char,sub} \cdot h_{sub} . \quad \textbf{(6)}$$

It is assumed that no energy is transferred to the surface by radiation. Finally the net heat flux entering the ablative material can be calculated as:

$$\dot{q}_{in} = \dot{q}_{conv,cb} - \dot{q}_{rad} - \dot{q}_{sub} . \quad \textbf{(7)}$$

2.2 Surface Recession

The surface recession is primarily determined by the surface temperature and the amount of oxygen diffusing to the surface. The mechanisms of surface ablation are oxidation and sublimation. It is assumed that only fully

pyrolysed material can be affected by surface recession. The removed material is pure carbon. According to [6] the quantitative amount of ablated carbon is determined from the experimental results of Metzger et. al. [7]. Equation (8) represents the mass flux of removed char normalized to the body radius r_b and the pressure of the boundary layer edge p_e. The resulting expression is only dependent on the surface temperature. K_0 and C are constants derived from the experiment and E and R are the activation energy and the universal gas constant respectively.

$$\dot{m}_{char}\sqrt{\frac{1.0133\cdot 10^5 r_b}{0.3048\cdot p_e}} = \frac{\sqrt{0.21}K_0 e^{-\frac{E}{RT_w}}}{\sqrt{\frac{0.3048}{r_b}+0.21\left(\frac{K_0}{C}\right)^2\left(\frac{e^{-\frac{E}{RT_w}}}{1+K\left(\frac{p_e}{1.0133\cdot 10^5}\right)^{-\frac{2}{3}}e^{-\frac{6.17\cdot 10^{-4}}{T_w}}}\right)^2}}. \tag{8}$$

Equation (8) is plotted in Figure 4. The surface mass flux is divided into 3 regions. For surface temperatures up to 1300 K the surface mass flux, and therefore the surface recession, increases with increasing temperature. This is due to the increasing reaction rate of the surface oxidation. This section is the rate-controlled regime. At temperatures above 1300 K the surface recession stagnates and remains constant up to a surface temperature of about 2000 K to 2500 K, depending on the pressure p_e. Even with increasing temperature, the surface oxidation remains constant because not enough oxygen reaches the surface by diffusion. This section is the diffusion-controlled regime. At higher temperatures, the surface mass flux increases further due to the onset of carbon sublimation. If there is combustion of pyrolysis gas and sublimated char, then less oxygen reaches the wall by diffusion and the diffusion-controlled mass flux has to be corrected. The stagnation pressure for the electromagnetic launched vehicle can reach up to 100 bar. This pressure region was not covered by the experiments in [7] so the data for these high pressures are extrapolated. This especially influences the sublimation controlled region.

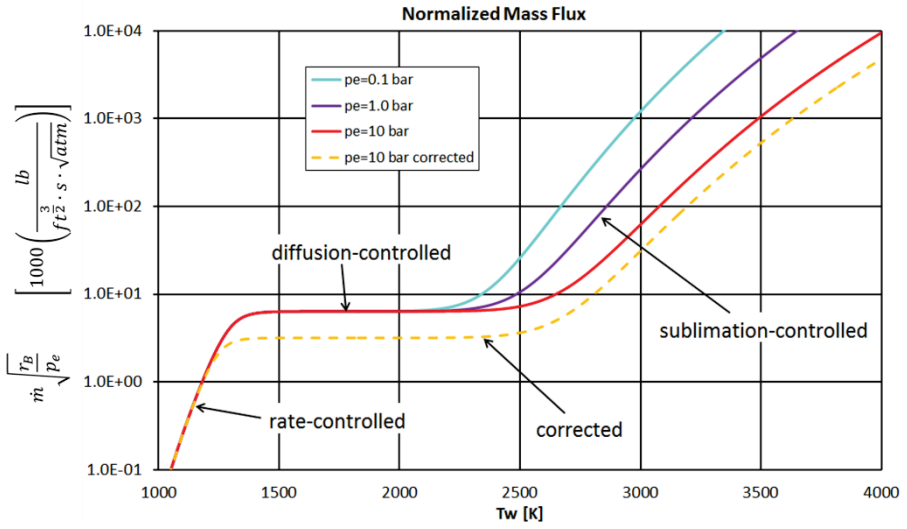

Figure 4: Surface Recession

To determine the amount of oxygen diffusing to the wall, the equation for the char mass flux in the diffusion controlled regime from [7] is used and the amount of oxygen needed for complete combustion of carbon to carbon monoxide is calculated:

$$\dot{m}_{ox,diff} = \frac{M_O}{M_C}\cdot 4.883\cdot 6.35\cdot 10^{-3}\sqrt{\frac{p_e\cdot 0.3048}{1.0133\cdot 10^5\cdot r_b}}. \tag{9}$$

The amount of oxygen that is required for complete combustion of pyrolysis gas and sublimated char can be calculated as:

$$\dot{m}_{ox,req} = \left(\frac{m_{ox}}{m_{gas}} \right)_{\Phi=1} \dot{m}_{gas} + \frac{M_O}{M_C} \dot{m}_{char,sub}, \tag{10}$$

$$\dot{m}_{char,sub} = \dot{m}_{char} - \frac{M_C}{M_O} \dot{m}_{ox,diff}. \tag{11}$$

If the amount of oxygen required for total combustion is greater than the amount of oxygen diffusing to the surface, the combustion will take place within the boundary layer and not at the surface. In this case no surface recession due to oxidation will take place; only the sublimation is enabled. (If the surface temperature is below the sublimation temperature, equation (11) will produce negative values and the result has to be set to 0.)
In case of surface combustion the amount of oxygen required for complete surface combustion (no oxygen consumption due to combustion of pyrolysis gas) must be determined:

$$\dot{m}_{ox,surf,req} = \left(\dot{m}_{char} - \dot{m}_{char,sub} \right) \frac{M_O}{M_C}. \tag{12}$$

This equals the rate-controlled or the diffusion-controlled mass flux, depending on the surface temperature. If the required amount of oxygen is greater than the amount of oxygen reaching the surface (due to consumption by combustion of pyrolysis gas), the diffusion-controlled mass flux has to be corrected:

$$\dot{m}_{char,diff} = \left(\dot{m}_{ox,diff} - \dot{m}_{ox,req} \right) \frac{M_C}{M_O}. \tag{13}$$

The total char mass flux can be calculated can be calculated as:

$$\dot{m}_{char} = \dot{m}_{char,diff} + \dot{m}_{char,sub}. \tag{14}$$

If more oxygen reaches the surface than required for ideal surface combustion, the mass flux is in the rate-controlled regime and can be simply calculated with equation (8).

2.3 Energy Equation

To solve the energy equation numerically, a one dimensional slice of the TPS and the base structure are divided into 1000 nodes and 20 nodes respectively. Due to the spherical shape of the assembly, the size of the nodes increases in outward direction (see Figure 5). This has to be considered in the equation.

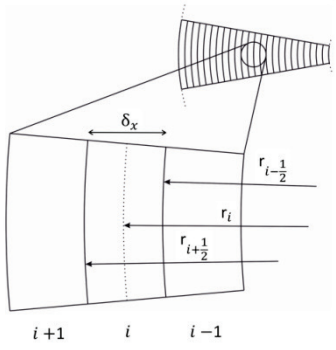

Figure 5: Numerical Grid

The change in temperature is evoked by heat conduction, heat flux due to pyrolysis reaction, and heat exchange with the pyrolysis gas streaming to the outer surface, and can be calculated as:

$$\frac{\partial T_i}{\partial t} = \frac{\left(\frac{r_{i+\frac{1}{2}}}{r_i}\right)^2 k_{i+\frac{1}{2}}(T,\rho)\cdot(T_{i+1}-T_i) - \left(\frac{r_{i-\frac{1}{2}}}{r_i}\right)^2 k_{i-\frac{1}{2}}(T,\rho)\cdot(T_i-T_{i-1})}{\rho_i \cdot c_{p,i}(T_i,\rho_i)\cdot\delta_x^2} + \frac{\dot{q}_{pyro,i}+\dot{q}_{gas,i}}{\rho_i \cdot c_{p,i}(T_i,\rho_i)\cdot\delta_x}. \quad \textbf{(15)}$$

The heat flux due to the pyrolysis reaction can be determined as following:

$$\dot{q}_{pyro,i} = \Delta h_{pyro}\frac{\partial \rho_i}{\partial t}\delta_x. \quad \textbf{(16)}$$

The pyrolysis heat flux is dependent on the rate of change of the density of the ablative material, which can be again calculated by following expression [8]:

$$\frac{\partial \rho_i}{\partial t} = -\rho_v\left(\frac{\rho_i-\rho_c}{\rho_v}\right)^2 \sum_{j=1}^{3} A_j e^{-\frac{Ej}{RT_i}}. \quad \textbf{(17)}$$

The sum expression represents the three major chemical reactions of the pyrolysis process; to calculate the reaction rate, these three processes have to be taken into account.
To calculate the heat flux due to heat transfer to the pyrolysis gas, it is assumed that the gas temperature and the ablative material are in thermal equilibrium in each node. Moreover the specific heat capacity of the pyrolysis gas is assumed to be constant. Therefore the heat flux can be determined as:

$$\dot{q}_{gas,i} = 0.5\cdot\dot{m}_{gas,i}\cdot c_{p,gas}\cdot(T_{i-1}-T_{i+1}). \quad \textbf{(18)}$$

The mass flux of the *i-th* node is the amount of pyrolysis gas produced in the node plus the gas entering from the preceding nodes:

$$\dot{m}_{gas,i} = \left(\frac{\partial \rho_i}{\partial t} + \sum_{j=1}^{i-1}\frac{\partial \rho_j}{\partial t}\left(\frac{r_j}{r_i}\right)^2\right)\delta_x. \quad \textbf{(19)}$$

The energy equation is solved for N nodes (comprising of the ablative material and the base structure), using an implicit scheme. The net heat flux entering the material (see equation (7)) cannot be modeled as a source term in the energy equation, because it is strongly dependent on the surface temperature. As the convective heat flux is of thermal diffusion type, an additional node $N+1$ is introduced, representing the conditions outside at the wall. The temperature of this node is set to the radiative-adiabatic wall temperature and the coefficient of heat transfer is set to a value that the net heat flux from equation (7) is achieved:

$$\alpha_{in,adj} = \frac{\dot{q}_{in}}{(T_{w,ad,rad}-T_w)}. \quad \textbf{(20)}$$

Therefore the correct heat flux enters the material, and the temperature cannot exceed the adiabatic wall temperature and the algorithm remains stable. The radiative-adiabatic wall temperature, at which convective and radiative heat flux are in equilibrium, can be calculated by numerically solving of the equation:

$$\alpha_{in,corr}\cdot(T_{R,corr}-T_{w,ad,rad}) = \sigma\cdot\varepsilon\cdot T_{w,ad,rad}^4. \quad \textbf{(21)}$$

Assuming that the blowing effect reduces the coefficient of heat transfer, the corrected coefficient of heat transfer can be calculated as following:

$$\alpha_{in,corr} = \frac{q_{conv}}{T_R - T_w}. \tag{22}$$

The nominal recovery temperature T_R is calculated with the equations of Fay and Riddell. Assuming that the combustion of pyrolysis gas and ablated char increases the recovery temperature, the corrected recovery temperature can be determined as:

$$T_{R,corr} = \frac{q_{conv,cb}}{\alpha_{in,corr}} + T_w. \tag{23}$$

The energy equation can be written in vector form:

$$\underline{y}_t = \underline{\underline{A}}\,\underline{y} + \underline{\varphi} \quad \text{with:} \quad \underline{y}_t = \begin{pmatrix} \frac{\partial T_1}{\partial t} \\ \vdots \\ \frac{\partial T_{N+1}}{\partial t} \end{pmatrix} \quad \underline{y} = \begin{pmatrix} T_1 \\ \vdots \\ T_N \\ T_{w,ad,rad} \end{pmatrix} \quad \underline{\varphi} = \begin{pmatrix} \frac{\dot{q}_{pyro,1} + \dot{q}_{gas,1}}{\rho_1 \cdot c_{p,1}(T_1,\rho_1) \cdot \delta_x} \\ \vdots \\ \frac{\dot{q}_{pyro,N} + \dot{q}_{gas,N}}{\rho_N \cdot c_{p,N}(T_N,\rho_N) \cdot \delta_x} \\ 0 \end{pmatrix}. \tag{24}$$

The matrix A is determined as:

$$\underline{\underline{A}} = \begin{pmatrix} -\gamma_{\frac{3}{2}} & \gamma_{\frac{3}{2}} & 0 & & & \\ \gamma_{\frac{3}{2}} & -\left(\gamma_{\frac{3}{2}} + \gamma_{\frac{5}{2}}\right) & \gamma_{\frac{5}{2}} & & & \\ & \ddots & \ddots & \ddots & & \\ & & \gamma_{i-\frac{1}{2}} & -\left(\gamma_{i-\frac{1}{2}} + \gamma_{i+\frac{1}{2}}\right) & \gamma_{i+\frac{1}{2}} & \\ & & & \ddots & \ddots & \ddots \\ & & & 0 & \gamma_{(N+1)-\frac{1}{2}} & -\gamma_{(N+1)-\frac{1}{2}} \end{pmatrix}, \tag{25}$$

with the matrix elements:

$$\gamma_{i\pm\frac{1}{2}} = \frac{r^2_{i\pm\frac{1}{2}} \cdot k_{i\pm\frac{1}{2}}(T,\rho)}{r_i^2 \cdot \rho_i(T_i) \cdot c_{p,i}(T_i) \cdot \delta_x^2} \quad i = 1..N-1, \quad \gamma_{N+\frac{1}{2}} = \gamma_{(N+1)-\frac{1}{2}} = \alpha_{in,adj} \cdot \delta_x. \tag{26}$$

Creating the average between two time steps, equation (24) can be rewritten as [9]:

$$\underbrace{\left(1 - \varepsilon \cdot \Delta t \cdot \underline{\underline{A}}\right)}_{\underline{\underline{B}}} \underline{y}_t = \underline{\varphi} + \underline{\underline{A}}\,\underline{y} \quad \varepsilon \in [0,1]. \tag{27}$$

Choosing ε=0.5 equation (27) represents the Crank-Nicolson method. The equation can be solved for y_t using the Thomas algorithm [9].

3. 6-DOF Model

The TPS model is coupled to a 6-DOF simulation model, to investigate the non-steady behaviour of the heat shield during the ascent. The model comprises of a flight mechanics module and aerodynamics model as well as guidance navigation and control simulation. Furthermore the vehicle configuration can be defined by a set of parameters, therefore arbitrary configurations can be simulated. This is important for optimization jobs.

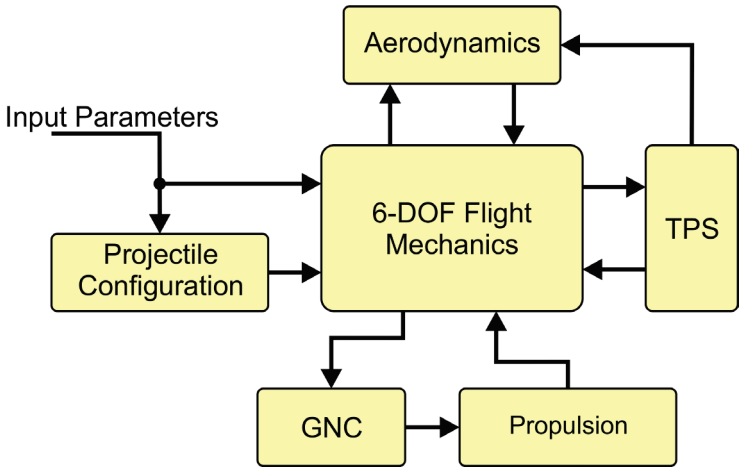

Figure 6: Simulation Model

4. Simulation

To validate the TPS model, the re-entry of the "Hayabusa" probe capsule is recomputed. The data for comparison was taken from [10]. The trajectory is approximated with two slopes for the altitude and three slopes for the velocity (see Figure 7). The simulation is done with a time offset of 50 s to the reference trajectory.

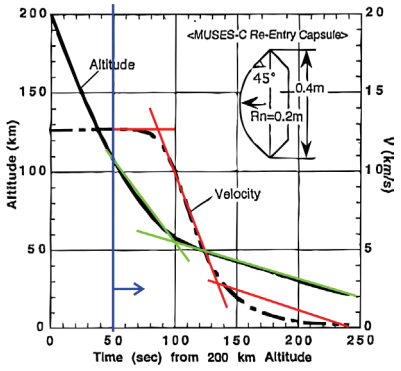

Figure 7: Hayabusa Trajectory [10]

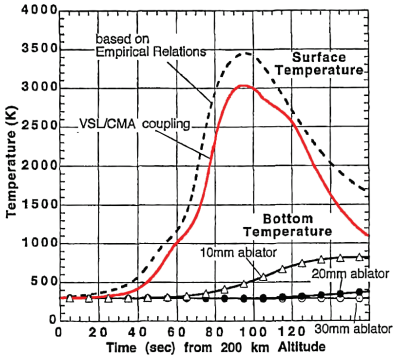

Figure 8: Surface Temperature [10]

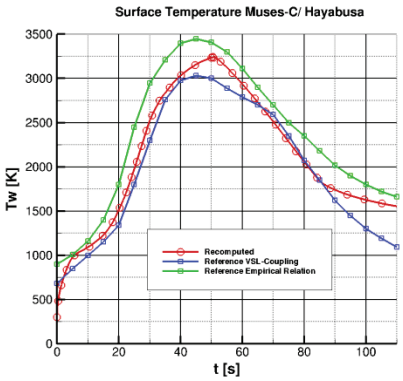

Figure 9: Recomputed Surface Temp.

The computed wall temperature (Figure 9) shows good agreement with the reference data from [10]. The surface temperature in the simulation after t=80 s decreases less than in the reference data. This is the point of intersection between the second and the third velocity slope. As the approximated velocity in this section is higher than the reference velocity, the surface temperature is also higher.

Figure 10 and Figure 11 show the layer evolution in the material cross-section. The penetration depth of the char layer shows good agreement with a value of about 4.5 mm. The penetration depth of the pyrolysis front in the simulation matches the reference data well. The surface recession in the simulation is only 0.5 mm in comparison to the reference with 1.0 mm. This is due to the lack of modelling of the oxygen consumption in the boundary layer due to combustion of pyrolysis gas in the reference case.

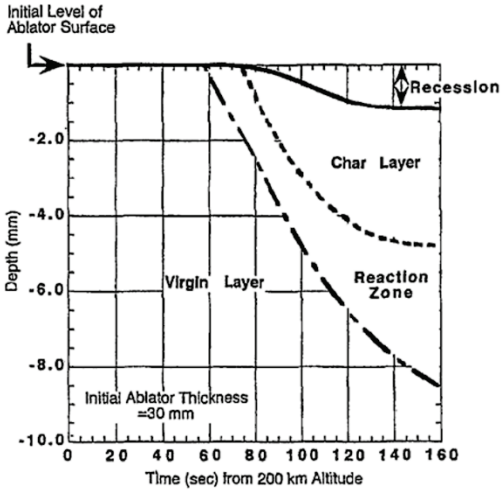

Figure 10: Hayabusa Layer Evolution [10]

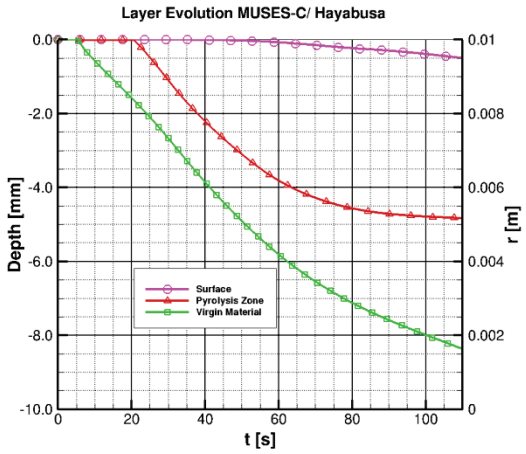

Figure 11: Recomputed Layer Evolution

Finally, with the coupled software, the ascent of an electromagnetically launched payload carrier is simulated. The projectile has a length of 7 m, a diameter of 0.32 m, and a mass of 500 kg. The thickness of the ablative heat shield is 15 mm at the stagnation point. The thickness of the base structure is 1.2 mm. The initial velocity is 3300 m/s and the vehicle is launched with an initial flight path angle of 50°. Figure 12 shows the complete flight profile to the desired low earth orbit. After the launch from the LRA, the projectile coasts up to 60 km, where the fairing is ejected. At an altitude of 80 km, the first stage ignites and further propels the vehicle. After another un-propelled coast phase, the second stage ignites and injects the payload carrier in a 300 km circular orbit. Figure 13 shows the first 30 s of the ascent, until fairing jettison. In the first 5 s of the flight the velocity decreases strongly. Thereafter the velocity slope is smaller. At lower altitudes, the Ma-number is about 9.5. It decreases to 8.0 at 60 km.

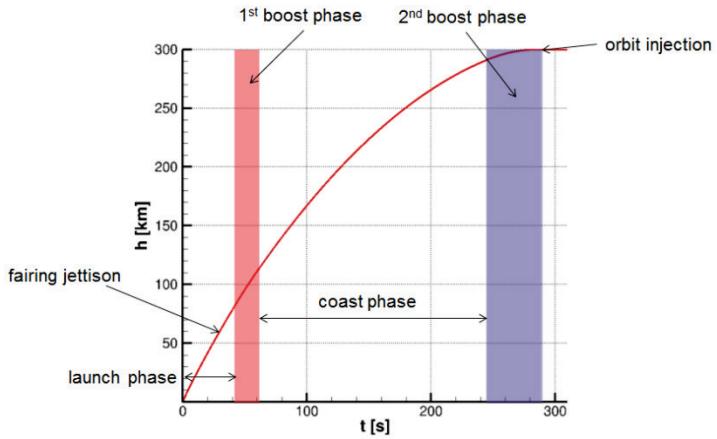

Figure 12: Flight Profile to Orbit

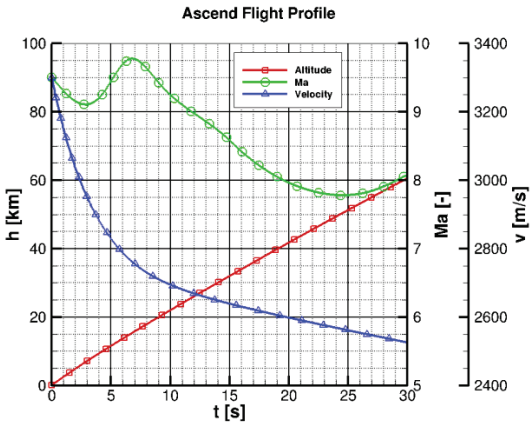

Figure 13: Flight through lower Atmosphere

Figure 14 shows the surface heat fluxes at the stagnation point. The initial convective heat flux has a very high peak of 6.5×10^7 W/m². With increasing altitude and decreasing velocity, the convective heat flux decreases as well. It is observed that the corrected heat flux (due to combustion and blowing) is higher than the cold wall heat flux. The additional heat flux due to combustion overcomes the cooling effect of blowing. Figure 15 shows the surface temperature and the stagnation pressure. According to the decreasing heat flux and the increasing altitude respectively, both values are decreasing strongly after launch. The peak surface temperature is about 3700 K.

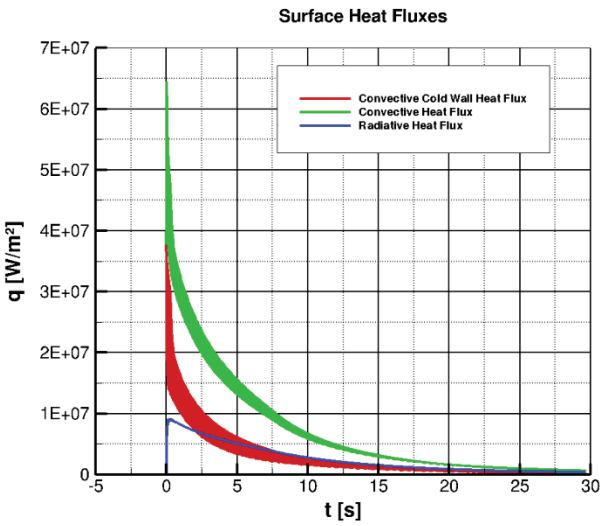

Figure 14: Surface Heat Fluxes

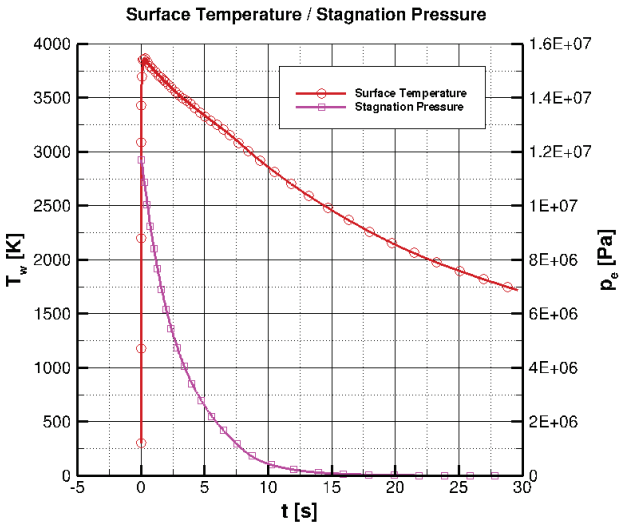

Figure 15: Surface Temperature and Stagnation Pressure

The layer evolution in the cross section of the material is shown in Figure 16. It is observed, that at the beginning of the flight, the char layer and the pyrolysis zone are consumed almost instantly due to the high heat flux and stagnation pressure. With decreasing load, the surface recession and pyrolysis reaction decreases as well, and a char layer and a pyrolysis zone are formed. Surface recession and char layer formation stops at about 28 seconds. Due to distribution of latent heat in the material, the pyrolysis layer further penetrates the material. The total surface loss is 6 mm, whereas the char layer has a thickness of roughly 1 mm. At fairing jettison, the remaining virgin material has a thickness of 6 mm.

In Figure 17 the temperature distribution in the material cross section at the stagnation point is shown. In the first seconds of the flight, a high temperature gradient is observed, moving deeper into the material with increasing surface recession. With decreasing heat load, the temperature gradient decreases as well and the latent thermal energy distributes in the material. Due to the short exposure time to high heat loads, the structure material does not heat up significantly, thus a good thermal protection is provided and the vehicle is capable to withstand the high thermal loads.

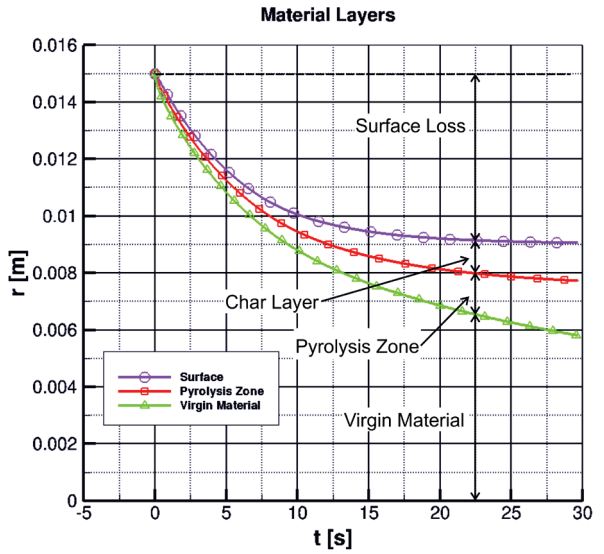

Figure 16: Material Layers

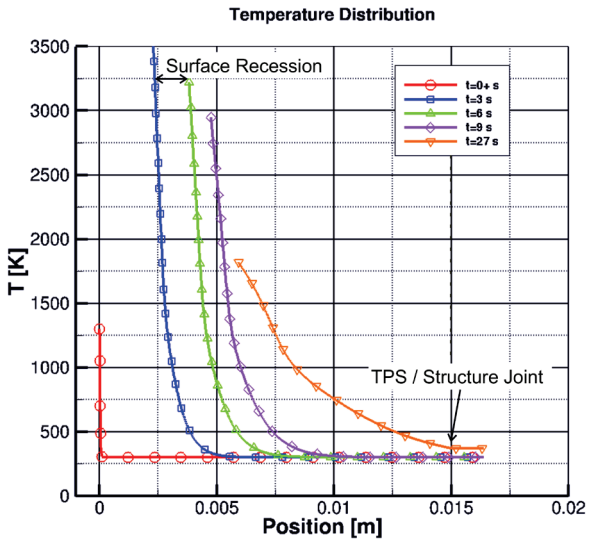

Figure 17: Temperature Distribution

5. Conclusion

To simulate a thermal protection system for an electromagnetically launched payload carrier that has to withstand very high thermal loads due to very high velocity at sea level, an ablative heat shield model is created that comprises of material response, aero-thermodynamics and boundary layer combustion modeling. It is a one dimensional engineering tool that avoids the use of CFD-techniques to enable fast calculations and to make the model suitable for optimization purpose. The TPS model is coupled to a 6-DOF flight mechanics module and to an aerodynamics module to compute a complete mission with all its aspects.

The model was verified using data of the "Hayabusa" space probe reentry calculation. The model shows good agreement with the reference data. Furthermore the ascent of an electromagnetically launched payload carrier was computed that is launched with an initial velocity of 3300 m/s at sea level. The results show that a 15 mm carbon phenolic heat shield at the stagnation point is sufficient to protect the vehicle against the high thermal loads. In the next step, the complete simulation model will be coupled to an optimization tool, to determine an optimal vehicle configuration for an electromagnetically launched projectile.

References

[1] Božić, O., Eggers, T., and Wiggen, S. 2011. Aerothermal and Flight Mechanic Considerations by Development of Small Launchers for Low Orbit Payloads Started from Lorentz Rail Accelerator. *3rd European Conference for Aero Space Sciences – EUCASS, 6-9 July 2009, Versailles-Paris, France, Progress in Propulsion Physics*, Vol. 2, (edited by L. DeLuca, C. Bonal, O. Heidn, S. Frolov,), *EUCASS advances in aerospace sciences book series, EDP sciences,* pp. 765-784, Torus Press.

[2] Schneider, M., Božić, O., and Eggers, T. 2011. Some Aspects concerning the Design of Multistage Earth Orbit Launchers using Electromagnetic Acceleration. 1*5th Electromagnetic Launch Symposium, May 17 - 20, 2010, Brussels, Belgium*. *IEEE Transaction of Plasma Science,* Vol. 39, Nr. 1, Part II, ISSN 0093-3813.

[3] Fay, J. A., and Riddell, F. R. 1958. Theory of Stagnation Point Heat Transfer in Dissociated Air. *Journal of Aeronautical Sciences*, Vol. 25, No. 2, pp. 73-85, 121.

[4] Marvin, J. G., and Pope, R. B. 1967. Laminar Convective Heating and Ablation in the Mars Atmosphere. *AIAA J.*, Vol. 5, No. 2.

[5] Hartnett, J. P., and Eckert, E. R. G. 1958. Mass Transfer Cooling with Combustion in a Laminar Boundary Layer. *Proceedings of the Heat Transfer and Fluid Mechanics Inst*., Stanford University Press, Stanford.

[6] Suzuki, K., Fujita, K., and Abe, T. 2003. Chemical Nonequilibrium Viscous Shock-Layer Analysis over Ablating Surface of Superorbital Re-Entry Capsule. *The Institute of Space and Astronautical Science Report*, SP No. 17.

[7] Metzger, J. W., Engel, M. J., and Diaconis, N. S. 1967. Oxidation and Sublimation of Graphite in Simulated Re-Entry Environments. *AIAA J.*, Vol. 5, No. 5.

[8] Clever, R. M., and Denny, V. E. 1975. Response of Charring Ablators to Severe Aerodynamic and Erosion Environments. *J. Spacecraft and Rockets*, Vol. 12, No. 9.

[9] Hoffmann, W. 2005. Differenzenverfahren für Partielle Differentialgleichungen. *Lecture Notes*. University of Hamburg.

[10] Suzuki, K. 2003. Trajectory-based Coupled Analysis of Viscous Shock Layer and Charring Material Ablation at Stagnation Point. *The Institute of Space and Astronautical Science Report*, SP No. 17.